Systematic Absences of Optical Phonon Modes in Phonon Dispersion Measured by Electron Microscopy

Aowen Li (李傲雯),[1] Paul M. Zeiger,[2] Zuxian He (何祖贤),[2] Mingquan Xu (许名权),[1] Stephen J. Pennycook,[1] Ján Rusz,[2,*] and Wu Zhou (周武)[1,†]

[1]School of Physical Sciences, University of Chinese Academy of Sciences, Beijing 100049, People's Republic of China

[2]Department of Physics and Astronomy, Uppsala University, Box 516, Uppsala 75120, Sweden

(Received 23 February 2024; accepted 10 June 2024; published 22 July 2024)

Phonon dispersion relations are widely used to elucidate the vibrational properties of materials. As an emerging technique, momentum-resolved vibrational spectroscopy in scanning transmission electron microscopy offers an unparalleled approach to explore q-dependent phonon behavior at local structures. In this study, we systematically investigate the phonon dispersion of monolayer graphene across several Brillouin zones (BZs) using momentum-resolved vibrational spectroscopy and find that the optical phonon signals vanish at the Γ points with indices $(hk0)$ satisfying $h + 2k = 3n$ (n denoted integers). Theoretical analysis reveals that the observed phenomena arise from the complete destructive interference of the scattered waves from different basis atoms. This observation, corroborated by the study of diamond, should be a general characteristic of materials composed of symmetrically equivalent pairs of the same elements. Moreover, our results emphasize the importance of multiple scattering in interpreting the vibrational signals in bulk materials. We demonstrate that the systematic absences and dynamic effects, which have not been much appreciated before, offer new insights into the experimental assessment of local vibrational properties of materials.

DOI: 10.1103/PhysRevLett.133.046101

Phonon dispersion relations are crucial for describing the phonon-mediated behavior of materials. However, measuring phonon dispersions at local structures remains challenging in most vibrational spectroscopy methods, such as optical spectroscopy [1–5], inelastic x-ray or neutron scattering (IXS or INS) [6–8] and high resolution electron energy-loss spectroscopy (HREELS) [9,10], which typically suffer from insufficient spatial or momentum resolution. For example, HREELS has been utilized to measure the surface phonon dispersion of epitaxially grown monolayer graphite, albeit with limited spatial resolution [11]. Recently, significant advances in monochromated scanning transmission electron microscopy (STEM) have provided a unique approach to directly assess the local vibrational properties of lattice imperfection and their correlation with the atomic structure [12–27]. Vibrational spectroscopy in STEM could balance the momentum, spatial, and energy resolution, enabling the detection of phonon modes and dispersion at structural imperfections [15,18,22,28–30]. It is worth noting that phonon dispersion obtained through momentum-resolved vibrational spectroscopy in STEM exhibits variable intensities along phonon branches and demonstrates different features on the same high-symmetry points in different Brillouin zones (BZs) [31]. The interpretation of such features should take into consideration the cross-section of inelastic electron scattering [28,29,32], which is not included in any calculations of only the phonon dispersion.

To probe the material properties using vibrational spectroscopy in STEM, it is necessary to establish a comprehensive understanding of the interaction between the incident electrons and crystal lattices. Several theoretical methods have been developed for this purpose [29,32–39]. In particular, the method derived from the Van Hove scattering formalism, originally designed for INS [40], has gained popularity for elucidating vibrational signals emerging at local structures [13,16,18,19]. The frequency-resolved frozen phonon multislice (FRFPMS) method, leveraging molecular dynamics and extending the frozen phonon approximation, offers inherently high computational efficiency and accommodates the effects of dynamical diffraction to interpret experimental vibrational intensities [30,31,41,42]. Complementary with theoretical simulation, Senga *et al.* discovered that vibrational signals in graphite and graphene vanish in the long-wavelength limit ($q \to 0$) because of the perfect screening of the ionic charge by the valence density in a semimetal [29]. However, since the perfect screening does not hold in a scattering process with a finite momentum transfer, the behavior of vibrational signals at the higher order Γ points

*Contact author: jan.rusz@physics.uu.se

†Contact author: wuzhou@ucas.ac.cn

is anticipated to differ from that observed at the central Γ point, thus deserving a comprehensive investigation.

Here, we employed momentum-resolved vibrational spectroscopy in STEM to investigate the vibrational signals within different BZs in monolayer graphene and diamond. The experiments were performed with a convergence semiangle of 3.5 mrad under 60 kV, resulting in a probe size of ∼1.2 nm and a diffraction spot radius of 0.45 $Å^{-1}$ [43]. Because of the extremely weak vibrational signals of single-layered graphene, especially within the momentum space beyond the first BZ, a slot-type EELS aperture with a collection range of 7×112 $mrad^2$ was used to facilitate high-efficiency parallel acquisitions along the Γ-*K*-*M*-*K*-Γ direction in momentum space [44]. It is also worth mentioning that a direct electron EELS detector was employed to eliminate readout noise in our data [45,46]. The energy resolution in the experiments is around 16 meV, sufficient to distinguish phonon modes in the acquired phonon dispersions. From these experimental conditions, we found that the optical phonon signals of graphene appear or disappear at different Γ points, forming a systematic pattern in momentum space. The consideration of cross-section of the inelastic scattering process within the Van Hove formalism unveils that the complete destructive interference of electron waves inelastically scattered by different basis atoms in the graphene unit cell results in the disappearance of the optical phonon signals at specific Γ points, indicating that this phenomenon should be a general characteristic of materials composed of symmetrically equivalent pair(s) of identical elements. This hypothesis is confirmed by our joint experimental and theoretical investigation to diamond, another phase of elemental carbon. The results for diamond also suggest that multiple scattering can further modulate the vibrational signals of bulk materials. Our study indicates that the systematic absences of optical phonon signals and dynamical effects are critical factors in the interpretation of vibrational spectroscopy, providing new insights into the study of vibrational properties of materials.

Figures 1(a) and 1(b) present two distinct experimental phonon dispersion diagrams of graphene (Fig. S1A [47]), collected at different regions in momentum space as indicated in Fig. 1(c). Notably, despite both being collected along the Γ-*K*-*M*-*K*-Γ direction in momentum space and correlated to the same vibrational modes in theory, these two diagrams exhibit different features. For example, in the upper panel of Fig. S1B, which displays the vibrational spectra extracted from the corresponding *M* points of these two phonon dispersion diagrams, the red curve shows a prominent peak corresponding to the transverse acoustic (TA) phonon mode, whereas the blue curve exhibits higher intensity within the region of longitudinal acoustic (LA), longitudinal optical (LO) and transverse optical (TO) modes. The disparities in spectral characteristics observed at the *M* and *K* points in graphene align with the calculated vibrational spectra of hexagonal boron-nitride (*h*-BN), as

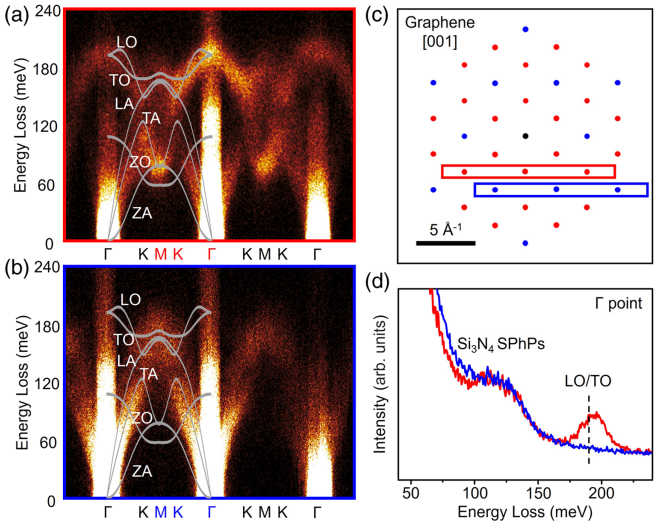

FIG. 1. Momentum-resolved vibrational spectroscopy of graphene at different momentum space regions. (a),(b) Experimental phonon dispersion diagrams of graphene, collected from the momentum spaces highlighted by red and blue rectangles in (c), respectively. (c) Schematic of graphene diffraction pattern along the [001] zone axis. The Γ points exhibiting or not exhibiting optical phonon mode signals are colored in red and blue, respectively. The central Γ point is shown in black. (d) Vibrational spectra extracted from the highlighted Γ points in (a),(b). The spectra extracted from (a) and (b) are colored in red and blue, respectively. The dashed line in this figure indicates the energy of the TO-LO phonon modes at the Γ points. The signals in the energy-loss range of 100–150 meV in the spectra of the Γ points are attributed to the surface phonon polaritons (SPhPs) of the Si_3N_4 substrate, labeled as Si_3N_4 SPhPs.

reported by two of the coauthors of this work [31], which can be explained by considering the scalar product of the phonon polarization vector of the vibrational modes ($\boldsymbol{e}$) and the momentum transfers of the inelastically scattered electrons ($\boldsymbol{q}$) using the scattering cross-section within the Van Hove formalism [29,32,40].

Regarding the Γ points [Fig. 1(d)], the red curve presents a prominent optical phonon peak at around 190 meV, while the blue curve lacks this feature. However, the variability in the visibility of vibrational signals at different Γ points cannot be attributed to the scalar product of $\boldsymbol{e} \cdot \boldsymbol{q}$ alone, because there is always at least one optical phonon branch that yields a nonzero scalar product $\boldsymbol{e} \cdot \boldsymbol{q}$, except at the central Γ point where $\boldsymbol{q}$ is zero. To explore the underlying mechanism governing the behavior of the optical phonon signals at the Γ points, we gathered a series of phonon dispersion diagrams collected from various momentum regions and checked the visibility of the signals in each diagram, as shown in Fig. S2 [47]. Based on the experimental findings and the sixfold structural symmetry inherent to graphene, a schematic in Fig. 1(c) denotes the Γ points in red or blue when the optical phonon peaks are visible or invisible, respectively, delineating a systematic pattern in momentum space.

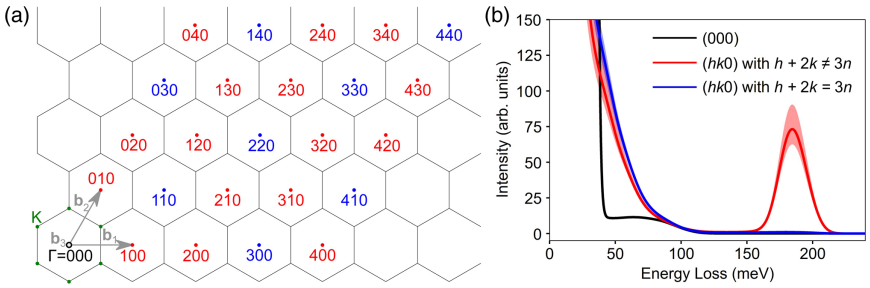

FIG. 2. Simulation of the graphene vibrational signals at different Γ points. (a) Reciprocal lattice of graphene along the [001] zone axis. The selected Γ points in the simulations are indexed. (b) Simulated vibrational spectra at the Γ points highlighted in (a). The black solid line visualizes the spectrum at (000), while the red and blue solid lines correspond to the mean spectra of their corresponding groups. The shaded region around the mean indicates the spread of the corresponding group as it traces the minimum and maximum intensities.

To understand our experimental observations, we conducted simulations of the vibrational spectra of graphene using the FRFPMS method with parameters identical to those in our experiments [31,41,47]. Figure 2 illustrates the chosen Γ points alongside their corresponding simulated vibrational spectra. In line with the notation employed in the experimental results, the simulated spectra from the red Γ points exhibited very strong optical phonon peaks, while the optical phonon signals in spectra from the blue Γ points almost vanish. The excellent agreement in the visibility of optical phonon signals at the Γ points between the simulated and experimental results is intriguing. Our results reveal that in monolayer graphene, the indices of Γ points $(hk0)$, where optical phonon peaks are invisible, should satisfy

$$h + 2k = 3n, \tag{1}$$

where h, k, and n are integers.

To elucidate the factors contributing to the systematic absences of the graphene optical phonon signals at different Γ points, we considered the double differential scattering cross-section within the Van Hove formalism [29,32,40]:

$$\frac{d^2\sigma}{d\Omega(\boldsymbol{q})dE} \propto \sum_{\nu} \frac{1 + \langle n(\boldsymbol{q}_0,\nu)\rangle_T}{\omega(\boldsymbol{q}_0,\nu)} \delta\big(\omega - \omega(\boldsymbol{q}_0,\nu)\big) \times \left| \sum_{\kappa} e^{-i\boldsymbol{G}\cdot\boldsymbol{R}_\kappa} e^{-W_\kappa(\boldsymbol{q})} f_\kappa^e(\boldsymbol{q}) \frac{\boldsymbol{q}\cdot\boldsymbol{e}_\kappa(\boldsymbol{q}_0,\nu)}{\sqrt{M_\kappa}} \right|^2, \tag{2}$$

where ν is the phonon band index, $\boldsymbol{q} = \boldsymbol{G} + \boldsymbol{q}_0$ is the momentum transfer of the incident electron, $\boldsymbol{G}$ is a reciprocal lattice vector and $\boldsymbol{q}_0$ is a vector in the first Brillouin zone, $\boldsymbol{R}_\kappa$ is the position of the κ th atom in the unit cell, $e^{-W_\kappa(\boldsymbol{q})} f_\kappa^e(\boldsymbol{q})$ is its associated thermally smeared scattering factor, and M_κ is its mass. Furthermore $\boldsymbol{e}_\kappa(\boldsymbol{q}_0,\nu)$ is the phonon polarization vector at the κ th atom in mode $(\boldsymbol{q}_0,\nu)$. It is notable that the two carbon (C) atoms in the unit cell of graphene have opposite phonon polarization vectors of the LO and TO modes at the Γ point ($\boldsymbol{e}_2 = -\boldsymbol{e}_1$), but identical thermally smeared scattering factor and the atomic mass. Thus, for optical phonon modes of graphene at Γ points, Eq. (2) can be expressed as follows:

$$\frac{d^2\sigma}{d\Omega(\boldsymbol{q})dE} \propto |\boldsymbol{q}\cdot\boldsymbol{e}_1(\boldsymbol{q}_0,\nu)|^2 |e^{-i\boldsymbol{G}\cdot\boldsymbol{R}_1} - e^{-i\boldsymbol{G}\cdot\boldsymbol{R}_2}|^2. \tag{3}$$

For both LO and TO branches, the first factor of Eq. (3) only vanishes at $\boldsymbol{G} = 0$, i.e., the central Γ point. At any other Γ point with $\boldsymbol{G} \neq 0$, at least one of the eigenvectors of these branches ν has a nonzero component along the momentum transfer $\boldsymbol{q}$, as we mentioned above.

The second factor of Eq. (3) has a similar form to the structure factor of graphene ($F_{\boldsymbol{G}} \propto e^{i\boldsymbol{G}\cdot\boldsymbol{R}_1} + e^{i\boldsymbol{G}\cdot\boldsymbol{R}_2}$) but with a minus sign between the waves scattered at the different basis atoms. By considering the indices of Γ points $(hk0)$ and the positions of the two basis atoms of graphene, the second factor of Eq. (3) can be rewritten as follows:

$$\left| e^{-i(h\boldsymbol{b}_1 + k\boldsymbol{b}_2)\cdot\boldsymbol{R}_1} - e^{-i(h\boldsymbol{b}_1 + k\boldsymbol{b}_2)\cdot\boldsymbol{R}_2} \right|^2 = 2\left[1 - \cos\left(\frac{2\pi(h+2k)}{3}\right)\right], \tag{4}$$

which equals zero when h and k satisfy $h + 2k = 3n$, where n is an integer (see Supplemental Material for derivation details [47]). This consideration of the double differential scattering cross-section demonstrates that complete destructive interference of excitations of optical phonons from different atomic sites takes place at the Γ points with indices satisfying $h + 2k = 3n$, thereby giving rise to the systematic absences observed in our experiments. This highlights an importance of interatomic cross-terms in the transition potential formulation of the inelastic phonon scattering, where such cross-terms have been considered negligible [37].

Based on the above derivation, we conclude that the symmetrically equivalent pair(s) of the same elements contributes significantly to the systematic absences in the optical phonon signals of graphene. However, for materials with dissimilar element pairs, their basis atoms have distinct weightings due to the variations in the magnitudes of their phonon polarization vectors, atomic masses, and thermally smeared scattering factor. Therefore, in such cases, instead of complete disappearance, a reduction in the intensity of the vibrational signals should be

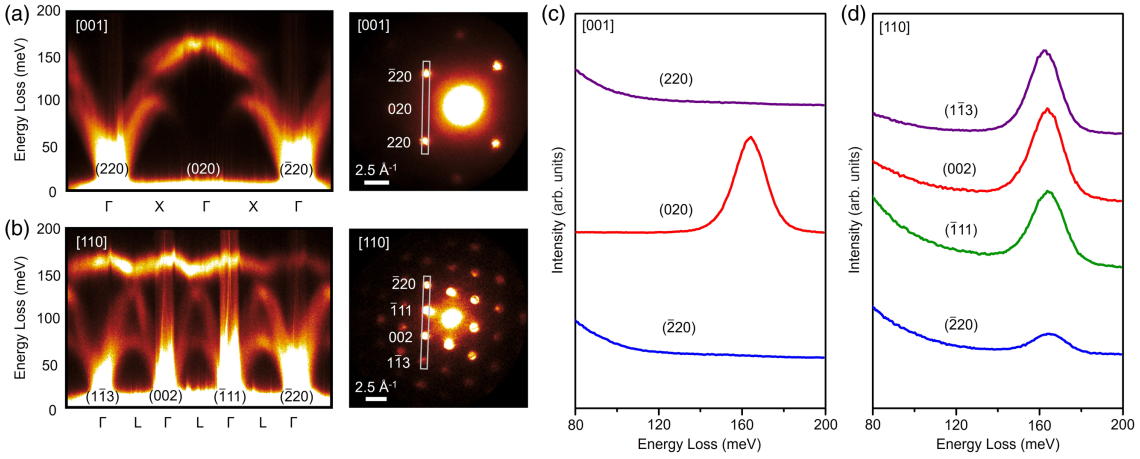

FIG. 3. Momentum-resolved vibrational spectroscopy of diamond. Phonon dispersions and diffraction patterns obtained along the (a) [001] and (b) [110] axes, respectively. The selected momentum space regions in the diffraction patterns are highlighted. (c) and (d) are the vibrational spectra extracted from the Γ points in (a) and (b), respectively.

expected, as shown in the simulated phonon dispersion of hexagonal boron nitride (*h*-BN) [31]. It should be mentioned that the discussion here is restricted to impact scattering and excludes any consideration of the SPhPs appearing at Γ points in experiment (Fig. S3) [57].

From the discussion above, it seems reasonable to infer that the systematic absences could also manifest in other materials that are composed of symmetrically equivalent pair(s) of the same elements, such as diamond. Diamond has a face-centered cubic lattice, composed of eight C atoms in its conventional cell with a two-atom basis. The phonon eigenvectors at the Γ points for the two C atoms in the basis are antiparallel. Applying the same derivation as we have employed for graphene, the systematic absences of optical phonon peaks in diamond are determined by the rule that $h + k + l = 4n$ (see Supplemental Material for derivation details [47]).

To verify our theory, we collected phonon dispersions of diamond on two different zone axes of [001] and [110] with sample thicknesses of 56 and 43 nm, respectively (Fig. S4 [47]). Along the [001] axis, the optical phonon signals at around 165 meV disappear at the $(\bar{2}20)$ and (220) spots but appear at the (020) spot, consistent with our theoretical derivation [Figs. 3(a) and 3(c)]. However, along the [110] axis, spectra collected at all Γ points present optical phonon signals, including the $(\bar{2}20)$ point that satisfies the $h + k + l = 4n$ rule [Figs. 3(b) and 3(d)]. Furthermore, we observed that the kinematically forbidden spot (002) is visible in our experimental diffraction pattern along the [110] axis, which was captured from the same sample region as for the phonon dispersion measurement, suggesting strong multiple elastic scattering in the thick diamond sample. Multiple scattering could explain the discrepancies between the experimental results and theoretical derivation of the visibility of the optical phonon peaks, as this factor is not included in the theory originating from the Van Hove formalism [40]. For example, in the [110] orientation, the optical phonon signals at the $(\bar{2}20)$ spot, which by the selection rule should vanish in diamond, can result from a combination of an inelastic scattering event to the $(\bar{1}11)$ spot and a subsequent elastic Bragg scattering event to the $(\bar{1}1\bar{1})$ spot. In contrast, introducing an optical phonon peak for the $(\bar{2}20)$ spot in the [001] orientation from such a combination of events from zero-order Laue zone (ZOLZ) diffraction spots is not feasible. The impact of multiple scattering involving excitation of spots from higher-order Laue zones (HOLZs) is negligible in practice, as evidenced by the different visibility of the kinematically forbidden spots in our experimental diffraction patterns along different orientations. Specifically, the (002) spot in the [110] orientation, which can be induced by a combination of elastic scattering events to spots from ZOLZ, shows strong contrast, while the (020) spot in the [001] orientation, which requires a combination from HOLZ, is almost invisible.

To confirm the role of multiple scattering in the visibility of the optical phonon peak at the $(\bar{2}20)$ point, we first performed FRFPMS simulations on a 50 nm thick diamond specimen (Fig. 4 and Fig. S5 [47]). FRFPMS includes the effects of dynamical diffraction along with the inelastic phonon scattering events. Therefore, if visibility of the optical phonon peak at the $(\bar{2}20)$ spot is indeed arising from multiple scattering, FRFPMS simulation should capture this behavior. As shown in the phonon dispersion [Fig. 4(a)] and the corresponding simulated spectra of the Γ points [Fig. 4(b)] in the [001] orientation, a clear and strong optical phonon peak (around 165 meV) appears at the (020) spot, while it becomes negligible at the (220) and $(\bar{2}20)$ spots. These results are highly consistent with our experiment, except that minuscule optical phonon peaks are present in the simulated spectra of the (220) and $(\bar{2}20)$ spots. These extremely weak optical phonon peaks at the (220) and $(\bar{2}20)$ spots, as well as the weak but nonzero intensity of the

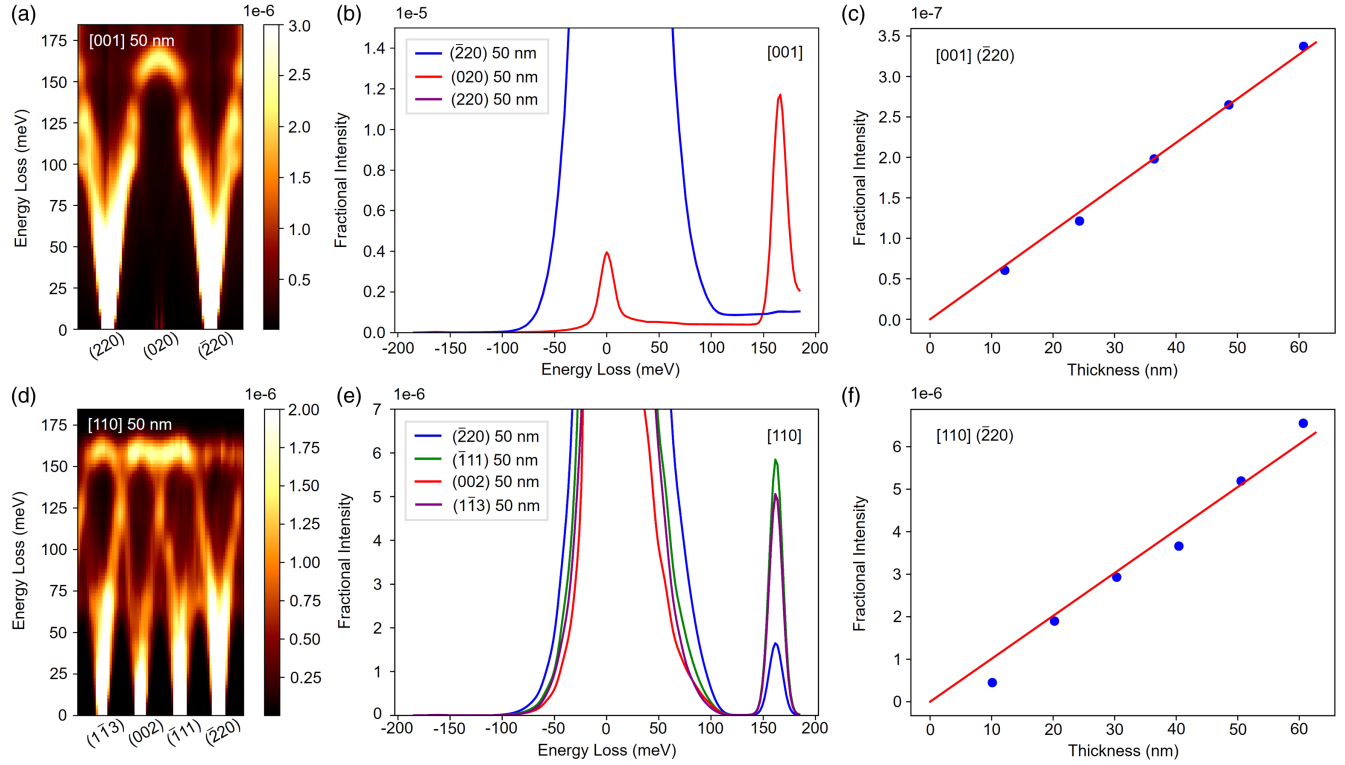

FIG. 4. Simulations of momentum-resolved vibrational spectroscopy of diamond. Simulated phonon dispersion plots for 50 nm thick samples in the (a) [001] and (d) [110] orientations. (b) and (e) are simulated spectra of Bragg spots corresponding to (a) and (d), respectively. (c) and (f) are the background-subtracted raw (unbroadened) fractional intensities of the optical phonon signals at the $(\bar{2}20)$ spot in the [001] and [110] orientations, respectively [59]. The red line in each panel is a linear fit of the data.

simulated zero-loss peak in the spectrum of the kinematically forbidden spot (020), should be attributed to multiple scattering events from HOLZs and are likely below detection limits in our experiments as we mentioned above. In the case of diamond [110] orientation, Figs. 4(d) and 4(e) show that the optical phonon peak intensities for the spots $(1\bar{1}3)$, (002), and $(\bar{1}11)$ are very similar, while the optical phonon peak at the $(\bar{2}20)$ spot is approximately 3 times lower, but still visible which is in agreement with experiment.

Furthermore, we have also simulated the phonon dispersions for diamond at other thicknesses in both [001] and [110] orientations. Given that the extinction distance of diamond at the (111) spot under 60 kV is approximately 38 nm [58], we should qualitatively expect nonlinear increases in the [110] orientation with varying sample thickness due to multiple scattering effects. This is exactly what our simulations show in Figs. 4(c) and 4(f): as sample thickness increases from 10 to 60 nm, the optical phonon signals at the $(\bar{2}20)$ spot remain small and increase linearly in the [001] orientation, while they exhibit significant intensities and nonlinear growth in the [110] orientation, highlighted by the deviations between the fractional intensities at different thickness and their linear fits. For instance, in the latter case, the signal intensity for a 10 nm thick sample is only 1/10th of that for a 50 nm thick sample. Hence, our experimental and simulated results demonstrate that dynamical effects should be considered when interpreting experimental vibrational spectroscopy data, especially for thick samples.

In summary, our systematic investigation of vibrational signals in graphene, complemented with theoretical analysis, has unveiled a phenomenon of systematic absences in optical phonon modes that originate from destructive interference of the inelastically scattered waves from different basis atoms. Furthermore, our analysis on diamond has confirmed these systematic absences at Γ points as a general characteristic in materials composed of symmetrically equivalent pair(s) of the same elements. The systematic absences also indicate that the vibrational signals of the same phonon modes from different BZs are not the same as those from the first BZ, which is usually neglected in the previous studies. Moreover, it is worth noting that the intensities of vibrational EELS in bulk samples are also modulated by dynamical effects, which is evidenced by the vibrational analysis on the diamond samples with a relatively large thickness. Our study demonstrates the importance of the systematic absences and dynamical effects in the modulation of the vibrational signals. Therefore, it is necessary to consider their impact on the variations of vibrational spectroscopy at the local structures of materials for a comprehensive understanding of their vibrational properties, especially for thick samples.

Acknowledgments—This research was supported by the Beijing Outstanding Young Scientist Program (BJJWZYJH012019144300039) and the CAS Project for Young Scientists in Basic Research (YSBR-003). We acknowledge the Swedish Research Council (Grant No. 2021-03848), Olle Engkvist's Foundation (Grant No. 214-0331), Knut and Alice Wallenberg Foundation (Grant No. 2022.0079), and STINT (Grant No. CH2019-8211) for financial support. The simulations were enabled by resources provided by the National Academic Infrastructure for Supercomputing in Sweden (NAISS) at NSC Centre partially funded by the Swedish Research Council through Grant Agreement No. 2022-06725. This research benefited from resources and support from the Electron Microscopy Center at the University of Chinese Academy of Sciences. We thank Dr. Tracy Lovejoy for valuable suggestions on momentum-resolved vibrational EELS experiments.

W. Z. conceived and supervised the project. A. L. carried out the momentum-resolved vibrational EELS experiments and data analysis with the help of M. X. M. X. and A. L. transferred the graphene sample and M. X. fabricated the diamond lamellas by FIB. P. Z., Z. H., and J. R. performed the FRFPMS simulations and developed the theoretical explanation of systematic absences of optical phonon peaks. A. L., P. Z., J. R., and W. Z. wrote the Letter with the input from M. X. and S. J. P. All authors discussed the results and commented on the manuscript.

[1] A. Lewis, H. Taha, A. Strinkovski, A. Manevitch, A. Khatchatouriants, R. Dekhter, and E. Ammann, Nat. Biotechnol. **21**, 1378 (2003).
[2] J. Olson, S. Dominguez-Medina, A. Hoggard, L.-Y. Wang, W.-S. Chang, and S. Link, Chem. Soc. Rev. **44**, 40 (2015).
[3] P. Verma, Chem. Rev. **117**, 6447 (2017).
[4] A. Dazzi and C. B. Prater, Chem. Rev. **117**, 5146 (2017).
[5] J. Lee, K. T. Crampton, N. Tallarida, and V. A. Apkarian, Nature (London) **568**, 78 (2019).
[6] E. Burkel, Rep. Prog. Phys. **63**, 171 (2000).
[7] N. Choudhury and S. L. Chaplot, Pramana **71**, 819 (2008).
[8] S. F. Parker, *in Encyclopedia of Biophysics*, edited by G. Roberts and A. Watts (Springer, Berlin, Heidelberg, 2019), p. 1.
[9] H. Ibach and D. L. Mills, *Electron Energy Loss Spectroscopy and Surface Vibrations* (Academic Press, New York, 1982).
[10] J. Li, J. Li, J. Tang, Z. Tao, S. Xue, J. Liu, H. Peng, X.-Q. Chen, J. Guo, and X. Zhu, Phys. Rev. Lett. **131**, 116602 (2023).
[11] C. Oshima and A. Nagashima, J. Phys. Condens. Matter **9**, 1 (1997).
[12] O. L. Krivanek *et al.*, Nature (London) **514**, 209 (2014).
[13] F. S. Hage, G. Radtke, D. M. Kepaptsoglou, M. Lazzeri, and Q. M. Ramasse, Science **367**, 1124 (2020).
[14] M. Xu *et al.*, Nat. Mater. **22**, 612 (2023).
[15] R. Qi *et al.*, Nat. Commun. **12**, 1179 (2021).
[16] X. Yan *et al.*, Nature (London) **589**, 65 (2021).
[17] Z. Cheng *et al.*, Nat. Commun. **12**, 6901 (2021).
[18] R. Qi *et al.*, Nature (London) **599**, 399 (2021).
[19] C. A. Gadre *et al.*, Nature (London) **606**, 292 (2022).
[20] E. R. Hoglund *et al.*, Nature (London) **601**, 556 (2022).
[21] X. Tian *et al.*, Sci. Adv. **7**, eabi6699 (2021).
[22] Y.-H. Li *et al.*, Proc. Natl. Acad. Sci. U.S.A. **119**, e2117027119 (2022).
[23] J. Kikkawa, T. Taniguchi, and K. Kimoto, Phys. Rev. B **104**, L201402 (2021).
[24] B. Haas, T. M. Boland, C. Elsässer, A. K. Singh, K. March, J. Barthel, C. T. Koch, and P. Rez, Nano Lett. **23**, 5975 (2023).
[25] E. R. Hoglund, D.-L. Bao, A. O'Hara, T. W. Pfeifer, M. S. Bin Hoque, S. Makarem, J. M. Howe, S. T. Pantelides, P. E. Hopkins, and J. A. Hachtel, Adv. Mater. **35**, 2208920 (2023).
[26] R. Senga, Y.-C. Lin, S. Morishita, R. Kato, T. Yamada, M. Hasegawa, and K. Suenaga, Nature (London) **603**, 68 (2022).
[27] N. Li *et al.*, Nat. Commun. **14**, 2382 (2023).
[28] F. S. Hage, R. J. Nicholls, J. R. Yates, D. G. McCulloch, T. C. Lovejoy, N. Dellby, O. L. Krivanek, K. Refson, and Q. M. Ramasse, Sci. Adv. **4**, eaar7495 (2018).
[29] R. Senga, K. Suenaga, P. Barone, S. Morishita, F. Mauri, and T. Pichler, Nature (London) **573**, 247 (2019).
[30] P. M. Zeiger and J. Rusz, Phys. Rev. B **104**, 094103 (2021).
[31] P. M. Zeiger and J. Rusz, Phys. Rev. B **104**, 104301 (2021).
[32] R. J. Nicholls, F. S. Hage, D. G. McCulloch, Q. M. Ramasse, K. Refson, and J. R. Yates, Phys. Rev. B **99**, 094105 (2019).
[33] L. J. Allen and T. W. Josefsson, Phys. Rev. B **52**, 3184 (1995).
[34] A. V. Martin, S. D. Findlay, and L. J. Allen, Phys. Rev. B **80**, 024308 (2009).
[35] B. D. Forbes, A. V. Martin, S. D. Findlay, A. J. D'Alfonso, and L. J. Allen, Phys. Rev. B **82**, 104103 (2010).
[36] N. R. Lugg, B. D. Forbes, S. D. Findlay, and L. J. Allen, Phys. Rev. B **91**, 144108 (2015).
[37] B. D. Forbes and L. J. Allen, Phys. Rev. B **94**, 014110 (2016).
[38] C. Dwyer, Phys. Rev. B **96**, 224102 (2017).
[39] P. Rez and A. Singh, Ultramicroscopy **220**, 113162 (2021).
[40] L. Van Hove, Phys. Rev. **95**, 249 (1954).
[41] P. M. Zeiger and J. Rusz, Phys. Rev. Lett. **124**, 025501 (2020).
[42] P. M. Zeiger, J. Barthel, L. J. Allen, and J. Rusz, Phys. Rev. B **108**, 094309 (2023).
[43] O. L. Krivanek, M. F. Chisholm, N. Dellby, and M. F. Murfitt, *in Scanning Transmission Electron Microscopy*, edited by S. J. Pennycook and P. D. Nellist (Springer, New York, 2011), p. 615.
[44] A. L. Bleloch *et al.*, Microsc. Microanal. **25**, 512 (2019).
[45] B. Plotkin-Swing *et al.*, Ultramicroscopy **217**, 113067 (2020).

[46] M. Xu, A. Li, S. J. Pennycook, S.-P. Gao, and W. Zhou, Phys. Rev. Lett. **131**, 186202 (2023).
[47] See Supplemental Material at http://link.aps.org/supplemental/10.1103/PhysRevLett.133.046101 for detailed methods and additional information. Supplemental Material also contains Refs. [48–56].
[48] X. Li *et al.*, Science **324**, 1312 (2009).
[49] S. Kim, S. Shin, T. Kim, H. Du, M. Song, C. Lee, K. Kim, S. Cho, D. H. Seo, and S. Seo, Carbon **98**, 352 (2016).
[50] C. Meyer, N. Dellby, J. A. Hachtel, T. Lovejoy, A. Mittelberger, and O. Krivanek, Microsc. Microanal. **25**, 122 (2019).
[51] R. F. Egerton, *Electron Energy-loss Spectroscopy in the Electron Microscope* (Springer, Boston, 2011).
[52] A. P. Thompson *et al.*, Comput. Phys. Commun. **271**, 108171 (2022).
[53] P. Rowe, V. L. Deringer, P. Gasparotto, G. Csányi, and A. Michaelides, J. Chem. Phys. **153**, 034702 (2020).
[54] J. Barthel, Ultramicroscopy **193**, 1 (2018).
[55] J. Tersoff, Phys. Rev. B **39**, 5566 (1989).
[56] J. Tersoff, Phys. Rev. B **41**, 3248(E) (1990).
[57] H. Yang, X. Yan, T. Aoki, and X. Pan, Microsc. Microanal. **28**, 2872 (2022).
[58] D. B. Williams and C. B. Carter, *Transmission Electron Microscopy* (Springer, Boston, 2009).
[59] C. G. Ryan, E. Clayton, W. L. Griffin, S. H. Sie, and D. R. Cousens, Nucl. Instrum. Methods Phys. Res., Sect. B **34**, 396 (1988).